FARADAY

# Quantum dynamical aspects of rotationally and vibrationally mediated photochemistry in matrices and at surfaces

## HCl/DCl in Ar and $NH_3/ND_3$ at Cu(111)

**Jörn Manz, Peter Saalfrank and Burkhard Schmidt**
*Institut für Physikalische und Theoretische Chemie, Freie Universität Berlin, Takustrasse 3, D-14195 Berlin, Germany*

We investigate two extensions of the concept of vibrationally mediated chemistry, from small molecules in the gas phase to small molecules in matrices and at surfaces using, as examples, the systems HCl/DCl in Ar and $NH_3/ND_3$ at Cu(111). The transition from isolated systems to the condensed phase calls for new quantum dynamical techniques and allows us to predict new phenomena. For matrix isolation, we propagate three-dimensional wavepackets representing photo-dissociated H or D atoms which penetrate from the initial cage into the lattice provided by the matrix. The cage-exit probabilities are found to depend not only on the initial vibrational, but also on the rotational states, owing to the environmental ($O_h$) symmetry provided by the (fcc) lattice of the matrix. As a consequence, we suggest the extension from vibrationally to rotationally, or rovibrationally mediated chemistry for matrix-isolated molecules. For molecules at surfaces, we adopt Gadzuk's jumping wavepacket plus incoherent averaging scheme, applied to an extended two-dimensional Antoniewicz-type model for the surface–molecule bond plus the vibrational coordinate which lends itself to preferential vibrational excitation (here the umbrella mode of ammonia). The desorption depends selectively on the initial vibrational state. As a consequence, we suggest the extension of traditional desorption induced by electronic transitions (DIET) to a vibrationally mediated IR–UV DIET scheme which may be used *e.g.* for enrichment of specific isotopomers at surfaces.

## 1 Introduction

Vibrationally mediated chemistry provides an important route to laser control of elementary chemical reactions.[1–17] By offering a possibility to control the efficiency of a reaction, it may be used to achieve either specific branching ratios of competing products, or selective reactivity of rather similar competing reactants, *e.g.* different isotopomers. The principle of vibrationally mediated chemistry is quite simple: essentially, the overall reaction is separated into two steps. First, the reactant is excited vibrationally in order to prepare a favourable precursor state, *e.g.* a local vibrational excitation of the bond to be broken, or of the isotopomer that should react exclusively. Second, this specific precursor state is converted into the desired product. Within this general concept of vibrationally mediated chemistry, there are, in principle at least, various possibilities, *e.g.* the initial vibrational excitation may be achieved by direct overtone or by IR multiple-photon absorption using continuous wave cw lasers or ultrashort (ps or sub-ps) IR laser pulses. Likewise, the second, reactive step may result from cw lasers, or ps/fs laser pulses, typically in the VIS or UV regimes, in order to induce a specific electronic transition and subsequent bond-selective photodissociation. Alternatively, the overall selectivity may be obtained by bimolecular reactions of vibrationally excited precursors. Moreover, both steps may be induced simultaneously, *e.g.* by cw lasers, or subsequently, *e.g.* by a series of laser pulses.

To the best of our knowledge, the concept of vibrationally mediated chemistry was first proposed by Letokhov.[1] Since then, it has developed into a flourishing field both experimentally[1–8] and theoretically.[9–17] In particular, selective photodissociation of different isotopomers, *i.e.* HBr *vs.* DBr by IR–UV cw lasers was first demonstrated by Zittel and Little.[2] Following systematic developments,[3] Crim and coworkers were the first to achieve vibrationally mediated IR–UV laser control of branching ratios in photodissociations, specifically for the reactions $HOD \rightarrow H + OD$ *vs.* $\rightarrow D + OH$[4] and $HNCO \rightarrow H + NCO$ *vs.* $\rightarrow HN + CO$.[5] Moreover, Crim *et al.* also demonstrated the first vibrationally mediated control of bimolecular reactions, specifically $H + HOD \rightarrow H_2 + OD$ *vs.* $\rightarrow HD + OH$.[8] From a theoretical point of view, it is gratifying that several of these important experimental demonstrations had already been predicted '*cum grano salis*' theoretically, see *e.g.* the papers by Shapiro *et al.*,[9] Schinke *et al.*[10] and Imre and Zhang[11] on the $HOD \rightarrow H + OD$ *vs.* $D + OH$ reaction, and by Kudla and Schatz for the $H + HOD \rightarrow H_2 + OD$ *vs.* $HD + OH$ reaction.[12] In turn, the experimental work[1–8] has also stimulated new theoretical investigations, see *e.g.* ref. 13–17.

Irrespective of the progress demonstrated in ref. 1–12, it should be noted that successful, *i.e.* consistent experimental and theoretical demonstrations of vibrationally mediated chemistry have been restricted to rather small molecules with two, three or, at most, four atoms. One reason is simply convenience, *i.e.* the pioneers in the field have wisely chosen rather simple systems in order to demonstrate the novel methods. Another reason may be much more fundamental, *i.e.* the selectivity of vibrationally mediated chemistry may decrease or even vanish in larger molecules because of competing processes, in particular intramolecular vibrational redistribution (IVR). Clearly, it is a challenge to verify vibrationally mediated chemistry in the condensed phase.

The purpose of this theoretical paper is to extend the field of vibrationally mediated chemistry, from small molecules to larger systems, and from gases to the condensed phase. For this purpose, our choice of systems has been motivated by the previous successes which have been documented for small molecules,[1–17] and by the requirement that competing processes in larger systems, such as IVR, should not destroy the overall selectivity. As a consequence, we consider small molecules which are coupled rather weakly to their environments.

Specifically, we develop new methods, and we present results for two types of systems, small molecules (i) in matrices and (ii) at metal surfaces, with applications to bond breaking or, in the case of surfaces, desorption in the model examples:
(i) HCl in Ar → H + Cl in Ar *vs.* DCl in Ar → D + Cl in Ar.
(ii) $NH_3$@Cu(111) → $NH_3$ + Cu(111) *vs.* $ND_3$@Cu(111) → $ND_3$ + Cu(111).

For these systems, we shall use rather simple models which allow us to describe some aspects of the quantum dynamics, and to predict new time-dependent phenomena of vibrationally mediated chemistry which have no analogues in the isolated molecules.

For example, in the vibrationally mediated photodissociation of small molecules in matrices, the kinetic energy of the H-atom photofragment, and hence the probability for cage exit, can be manipulated by vibrational pre-excitation of HCl. The yield of photodissociation should also depend on the relative orientation of the molecule in the original cage of the matrix. We shall investigate, therefore, the possibility to extend the concept of vibrationally to ro-vibrationally mediated chemistry in order to control the photodissociation yield, not only *via* the intermediate vibrational excitation but also *via* specific rotational states with favourable orientations.

In the case of adsorbates at surfaces one aspect is the desorption of specific isotopomers, *i.e.* one isotopomer should leave, the other should stay at the surface, yielding selective isotopomer enrichment at surfaces. For this purpose, we shall suggest another extension of vibrationally mediated chemistry, *i.e.* selective excitations of vibrations of the adsorbate which should enhance the rate of breaking of the surface–adsorbate bond. To some extent, this process implies the flux of energy from one vibrational degree of freedom (the molecular one) to another (the molecule–surface bond), *i.e.* restricted IVR, which supports selectivity of the overall process instead of diminishing it.

## 2 Vibrationally mediated photochemistry in matrices

### A Introduction

Photodissociation of small molecules in rare-gas matrices can be regarded as a prototype system for molecular dynamics in solids. The main solvent effect on photodissociation dynamics is the cage effect which delays, or even prevents, permanent bond breaking of the fragments.[18] In principle, direct cage exit is only possible if the photofragment is much smaller than the matrix atoms and if the excess energy of the fragment is sufficient to overcome the barrier induced by the cage atoms. The process of direct cage exit can occur either immediately following the excitation, or after one (or more) unsuccessful tries (delayed exit). The opposite extreme to direct cage exit (be it delayed or not) is indirect cage exit, in which a fragment significantly distorts the cage by collisional energy transfer, thus opening new 'windows' in the cage walls. In the present investigation we want to confine ourselves to the process of direct cage exit. Naturally, this process is limited to the smallest photofragments. Apart from one study of $F_2$ in Ar giving evidence for direct cage exit,[19] sudden cage exit is considered as a possible pathway mainly for hydrogen photofragments. There are numerous experimental[20–22] and theoretical[23–25] studies of hydrogen halides and of dihydrides discussing the issue of direct *vs.* indirect and immediate *vs.* delayed cage exit as a function of the excess energy.

A challenging question in the study of photofragment dynamics in rare-gas matrices is the importance of quantum effects. Such effects are expected to play a dominant role for processes where light atoms are involved. However, almost all the theoretical treatments mentioned above[21,24,25] rely on many-particle classical trajectory simulations. One notable exception, demonstrating the importance of tunnelling and zero-point energy is a study of HI in Xe, where the H atom wavefunction is modelled by distributed Gaussian wavepackets.[26] Another example is a linear model of $I_2$ in Ar.[27] Here, we present a first three-dimensional treatment of H-atom photofragment quantum dynamics in a rare-gas environment. As a model system we choose HCl in Ar which has recently been investigated both experimentally[22] and theoretically[25] and which is especially amenable to simulations owing to the simple interaction potentials and the small number of electronic states involved.

Our special focus will be on the dependence of photodissociation dynamics on the initial rovibrational quantum state of the matrix-isolated molecule. First, the main effect of vibrational pre-excitation is the larger Franck–Condon region of the electronic excitation to a repulsive state which results, according to a reflection principle, in a wider distribution of kinetic energies of the photofragments. Because the immediate cage exit depends critically on the crossing of potential barriers, the kinetic energy of the photofragments is one of the key aspects of cage exit.

Second, for matrix-isolated molecules the initial angular distribution of orientations of the guest molecule with respect to the lattice is expected to be of importance. Experimental evidence stems from anomalous temperature effects observed in studies of $Cl_2$ in Xe,[28] $F_2$ in Kr[29] and $O_3$ in Ar[30] which are orientationally locked at very low temperatures. Owing to the onset of librations or rotations, substantial changes in the quantum yield of photodissociation could be observed upon increasing the temperature. Although hydrogen halides, such as the HCl molecule to be investigated here, are known to rotate almost freely in matrices, some orientational effects were recently predicted for HCl in Ar,[31] based on an analysis of rotational wavefunctions for this system which will be investigated further in the present work.

### B Model and potentials

Here we only give a brief outline of the methods employed; for a more, detailed description we refer to a forthcoming publication.[32] Our model consists of an HCl molecule occupying a mono-substitutional site in an otherwise perfectly symmetric fcc crystal of Ar. This assumption can be justified by the comparable van der Waals radii of HCl and Ar. The environment of the guest molecule is of octahedral symmetry and is modelled by 10 shells of Ar atoms: 12 nearest neighbours along the ⟨110⟩ directions, 6 second-nearest neighbours along the ⟨100⟩ directions, *etc.*

In order to describe the dynamics of HCl photodissociation, the Cl atom and the Ar atoms are assumed to be frozen in their equilibrium position. The dynamics of the H atom is represented by a three-dimensional wavefunction. In analogy to the close-coupled-wave-packet (CCWP) approach common in diatom scattering theory,[33] the wavefunction can be written in polar coordinates

$$\psi^{(i)}(r, \Theta, \phi) = \sum_{J=0}^{\infty} \sum_{n=0}^{g_i(J)} r\chi_{Jn}^{(i)}(r) Z_{Jn}^{(i)}(\Theta, \phi) \qquad (1)$$

where the angular dependence is expanded in symmetry adapted spherical harmonics (surface harmonics) of the $i$th irreducible representation of the octahedral point group $O_h$

$$Z_{Jn}^{(i)}(\Theta, \phi) = \sum_{m} c_{Jnm}^{(i)} y_{Jm}^{(i)}(\Theta, \phi); \quad n = 0 \cdots g_i(J) \qquad (2)$$

which are obtained by projection techniques[34] and where $g_i(J)$ gives the number of different surface harmonics for a given angular momentum $J$ and a given representation $i$. Note that the computational effort is reduced substantially by introduction of surface harmonics owing to the large number of vanishing $g_i(J)$.

Initially, the HCl molecule is in its electronic ground state. Neglecting vibration–rotation coupling, the radial part $r\chi(r)$ of

the wavefunction is taken to be an eigenfunction of a Morse oscillator representing the ground-state potential ($^1\Sigma$). The angular part of the time-independent Schrödinger equation is solved by diagonalization of the matrix

$$(\hat{H})^{(i)}_{JnJ'n'} = \frac{J(J+1)}{2mr_v^2}\,\delta_{JJ'}\,\delta_{nn'} + V^{(i)}_{JnJ'n'} \qquad (3)$$

where $m$ is the hydrogen mass and $r_v$ is the vibrationally averaged bond length of the hydride. The potential matrix elements

$$V^{(i)}_{JnJ'n'} = \int_0^{\pi} \sin\,\Theta\,\mathrm{d}\Theta \int_0^{2\pi} \mathrm{d}\phi\,[Z^{(i)}_{J'n'}(\Theta,\phi)]^* V(\Theta,\phi) Z^{(i)}_{Jn}(\Theta,\phi) \qquad (4)$$

are obtained by numerical integration of the guest–host potential function $V(\Theta, \phi)$ which is the pairwise sum of anisotropic Ar–HCl potentials of spectroscopic accuracy.[35]

The process of electronic excitation is modelled by instantaneously promoting the HCl molecule to the excited $^1\Pi$ state. The solution of the time-dependent Schrödinger equation for the *ansatz* (1) then yields the following set of coupled equations

$$i\hbar\frac{\partial}{\partial t}[r\chi^{(i)}_{Jn}(r)] = -\frac{\hbar^2}{2m}\frac{\partial^2}{\partial r^2}[r\chi^{(i)}_{Jn}(r)] + \frac{J(J+1)}{2mr^2}[r\chi^{(i)}_{Jn}(r)] + \sum_{J'n'} V^{(i)}_{JnJ'n'}(r)[r\chi^{(i)}_{J'n'}(r)] \qquad (5)$$

The $r$-dependent potential matrix elements are obtained as given in eqn. (4) but with $V(r, \Theta, \phi)$ consisting of the repulsive HCl ($^1\Pi$) potential[36] and the pairwise sum of H–Ar potentials obtained from scattering experiments.[37] The partial differential equations are solved numerically using a Fourier collocation scheme[38] for discretization in the radial coordinates. We use 512 grid points covering the range from 0.05 to 1.1 nm, with a negative imaginary potential damping the wavefunction on the last 50 grid points. The expansion of the angular part of $\Psi$ in surface harmonics is found to be converged at $J_{max} = 16$. The time-evolution operator is evaluated by expansion in Chebychev polynomials[38] with a time step of 5 fs.

### C Initial state rotational wavefunctions

The main effects of the matrix on the wavefunction $\Psi(r, \theta, \phi)$ of the electronic ground state of matrix-isolated molecules are orientational effects. Hence, we concentrate on rotational wavefunctions of HCl/DCl in Ar. Note that matrix-induced vibrational frequency shifts are very small (of the order of 1%) and have been published elsewhere.[39] Table 1 summarizes the rotational energy levels and Fig. 1 shows the wavefunctions obtained by diagonalization of eqn. (3).

Although the potential-energy function has a notable anisotropy with an energy difference of *ca.* 30 $cm^{-1}$ between the maxima (along ⟨110⟩) and minima (along ⟨111⟩), the lowest rotational states are almost identical to the pure $J = 0$ ($A_{1g}$) and $J = 1(T_{1u})$ states of a free molecule with a rotational constant of 10.3 $cm^{-1}$ (HCl) or 5.3 $cm^{-1}$ (DCl). This surprising behaviour of the rotational wavefunction is due to the uncertainty principle: A wavefunction that fitted the undulation of the potential (here $J = 4$) would be much higher in kinetic energy because of the stronger localization in space. Hence, the barriers which are of the order of 3 or 6 rotational constants for HCl or DCl, respectively, cannot hinder the rotation of the molecule substantially. By analogy with crystal field theory, all levels for $J \geqslant 2$ are split by the external octahedral field. The $J = 2$ level is split into an $E_g$ and $T_{2g}$ sublevel, the $J = 3$ level is split into $A_{2u}$, $T_{1u}$ and $T_{2u}$. The

**Table 1** Rotational energy levels of HCl and DCl in Ar matrix (vibrational ground state)

| $J$ | irrep. | HCl | DCl | orientation |
|---|---|---|---|---|
| 0 | $A_{1g}$ | 0.00 | 0.00 | isotropic |
| 1 | $T_{1u}$ | 2.00 | 2.00 | ⟨100⟩ |
| 2 | $E_g$ | 5.79 | 5.62 | ⟨100⟩ |
| 2 | $T_{2g}$ | 6.13 | 6.24 | ⟨110⟩ |
| 3 | $A_{2u}$ | 11.88 | 11.17 | ⟨111⟩ |
| 3 | $T_{1u}$ | 11.73 | 11.52 | ⟨111⟩, ⟨100⟩, ⟨110⟩ |
| 3 | $T_{2u}$ | 12.32 | 12.61 | ⟨110⟩ |

The energies are given in units of the rotational constant of $B = 10.3$ and $B = 5.3$ $cm^{-1}$ for HCl and DCl, respectively.

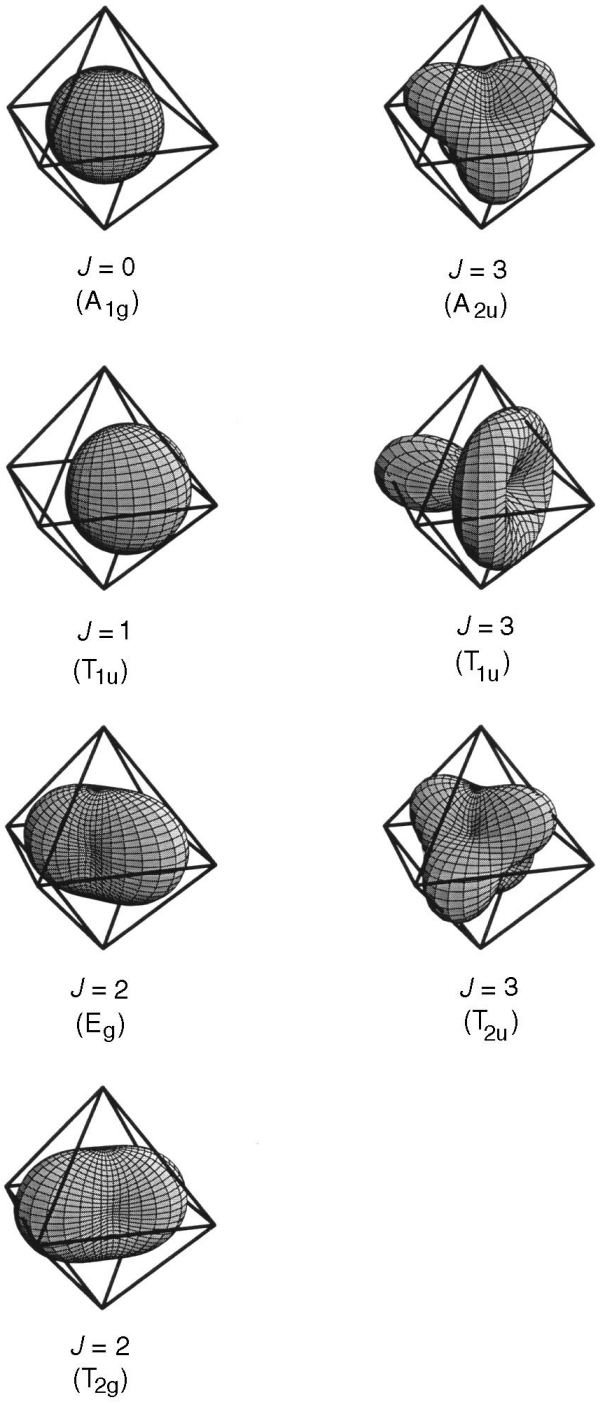


**Fig. 1** Rotational wavefunctions for the electronic ground state of HCl in Ar (fcc). The angular dependence of the first seven states is superimposed on a sphere. The circumscribed octahedra are oriented with their corners along the crystallographic ⟨100⟩ axes.

$T_{2g}$–$E_g$ splitting has been measured only for the system DCl/Ar.[40] The experimental value of 2.6 $cm^{-1}$ is in reasonable agreement with our value of 3.3 $cm^{-1}$.

A comparison of the HCl and DCl data in Table 1 shows an interesting isotope effect. The splitting of the $J = 2$ and $J = 3$ level in units of the rotational constant is much larger for HCl than for DCl. The reason for this is the nature of the rotational eigenstates, which can be seen from an analysis of the eigenvectors of the matrix (3). Although the rotational wavefunctions are almost identical to single-surface harmonics, as implied by the labelling with $J$ levels, there is some tiny admixture of surface harmonics corresponding to higher $J$ states. For example, the coefficients of the lowest state of HCl are 0.9998 for $J = 0$, 0.0153 for $J = 4$, and 0.0126 for $J = 6$. For DCl the latter two coefficients are twice as large. This can be understood in terms of the kinetic energy. Because the energy of pure $J$ states scales inversely with the reduced mass, there will be a larger proportion of higher-$J$ states for the heavier isotopes. Similarly, the different splitting of the $J = 2$ and $J = 3$ states of HCl and DCl is also caused by the different coefficients of higher-$J$ states.

The most interesting feature of the rotational wavefunction is the angular distribution of orientations of the molecule with respect to the crystallographic axes (see Fig. 1). The orientation of the maxima of probability is given in the last column of Table 1. The distribution of the $J = 0$ state is isotropic, the $J = 1$ ($T_{1u}$), $J = 2$ ($E_g$) and $J = 3$ ($T_{1u}$) wavefunctions are peaked along the $\langle 100 \rangle$ direction pointing towards the second-nearest neighbours. In contrast, the $J = 2$ ($T_{2g}$) and $J = 3$ ($T_{2u}$) distributions exhibit maxima along the nearest-neighbour $\langle 110 \rangle$ directions. Only the $J = 3$ ($A_{2u}$) wavefunction shows a maximum in the $\langle 111 \rangle$ direction which is known to be the preferred pathway for direct cage exit.[24] In the following section we will investigate how the probability of direct cage exit depends on the initial rotational state.

### D Wavepacket dynamics

The CCWP wavepacket dynamics of the photodissociation process of HCl in Ar is illustrated in Fig. 2. Here, we restrict ourselves to totally symmetric wavefunctions, which transform according to the totally symmetric representation $A_{1g}$ of the octahedral point group $O_h$. For this irreducible representation the only existing surface harmonics are those for $J = 0, 4, 6, 8, \ldots$ as shown in the left column of the figure. The right column shows the time dependence of the corresponding radial wavefunctions $r\chi_J(r)$ which are obtained from the coupled differential equations (5).

For reference, we consider, first, the case of direct photodissociation. Here, the initial H-atom wavepacket is assumed to be a direct product of the vibrational ground state $v = 0$ of the $^1\Sigma$ potential and the isotropic rotational ground state which is essentially a $J = 0$ state. The wavepacket, which starts at an internuclear distance of $r = 0.127$ nm, moves outwards owing to the strong HCl repulsion of the $^1\Pi$ state. After 7 to 8 fs it reaches a repulsive wall at $r \approx 0.25$ nm. This repulsion is induced by the 12 nearest-neighbour atoms of the fcc lattice, which are located on the centres of the edges of the octahedron. Here, the wavepacket bifurcates for the first time. Some part of the probability amplitude is reflected by the first coordination shell and is confined to rattling oscillations within the cage, while another part of the wavefunction leaves the cage directly and diffuses into the Ar lattice. As time proceeds we see further bifurcation and interference until the wavefunction becomes essentially structureless at $t \approx 50$ fs.

As a consequence of the off-diagonal elements of the potential matrix in eqn. (5), some probability is transferred into higher-$J$ states. The radial functions for $J = 4$, 6, 8 show the build-up of a wavepacket on a timescale of *ca.* 5 fs. The direct relationship between the geometry of the angular wavefunction and the cage exit probability can be seen very clearly: The $J = 4$ surface harmonic which is strongly pre-aligned along the $\langle 100 \rangle$ direction, passes the first coordination shell almost completely. After 15 fs it hits the second shell and is reflected by the six second-nearest-neighbour atoms located on the corners of the octahedron. In contrast, the $J = 6$ wavefunction which has extrema along the $\langle 100 \rangle$, $\langle 110 \rangle$ and $\langle 111 \rangle$ orientations is almost completely reflected by the cage formed by the nearest neighbours. The surface harmonic for $J = 8$ (and similarly for even higher ones) has already so many extrema, that the time dependence of the radial wavefunction closely resembles that of the purely isotropic $J = 0$ state.

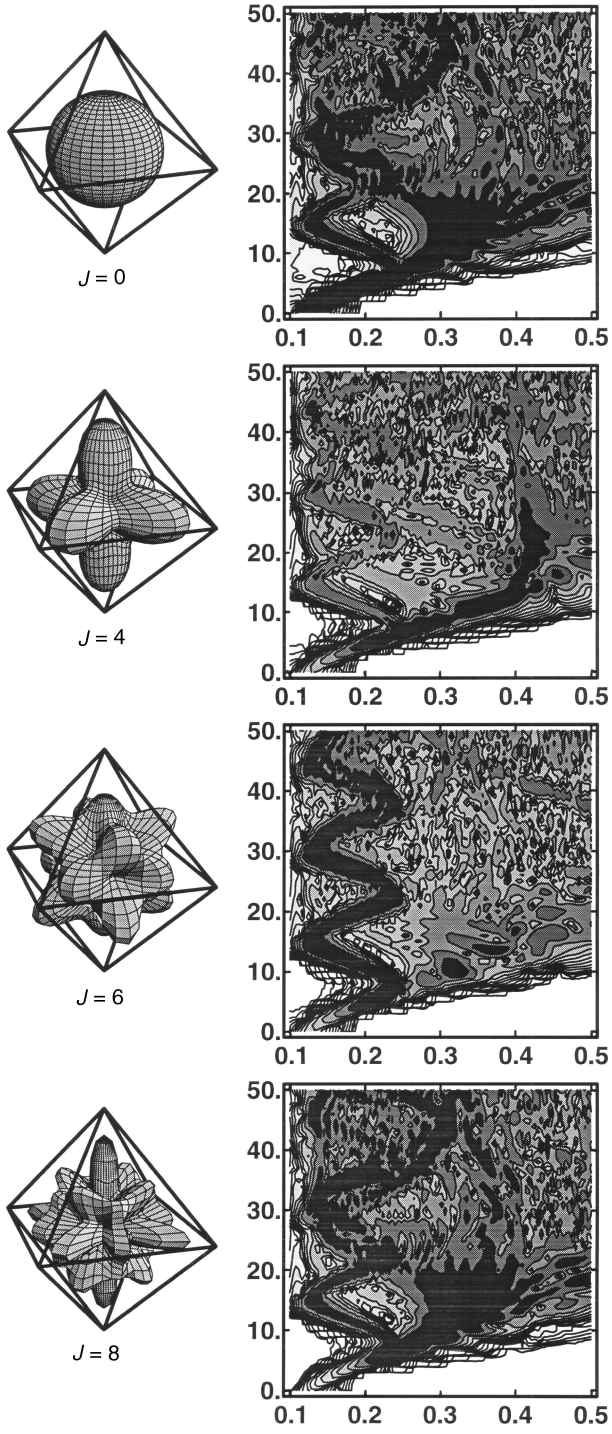


**Fig. 2** Wavepacket dynamics of photodissociation of HCl ($v = 0$, $J = 0$) in Ar. The left column shows the four lowest surface harmonics $Z_J(\Theta, \phi)$. The right column shows contours of the modulus of the corresponding radial functions $|r\chi_J(r)|$. The abscissa gives the H—Cl distance in nm, the ordinate gives the time in fs.

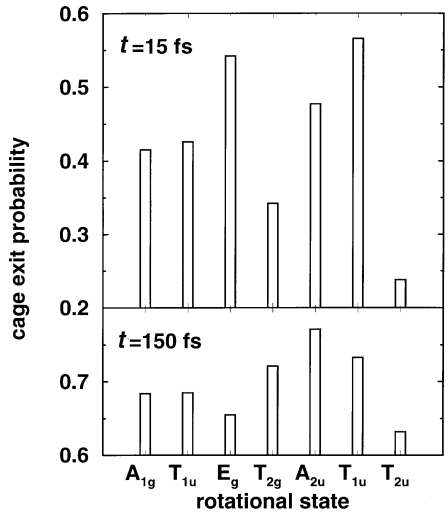


**Fig. 3** Immediate ($t$ = 15 fs) and delayed ($t$ = 150 fs) cage-exit probability of HCl ($v = 0$) in Ar (fcc) matrix as a function of the initial rotational state

### E Cage-exit probability

In our simulations the cage-exit probability is the probability for finding the hydrogen photofragment outside a sphere of radius $r_{NN}$

$$P^{(i)}(t) = \sum_{Jn} \int_{r=r_{NN}}^{\infty} dr\, r^2 |\chi_{Jn}^{(i)}(r, t)I^2 \quad (6)$$

where $r_{NN} = a/\sqrt{2}$ is the nearest-neighbour distance and $a$ is the lattice constant of Ar(fcc).

In the following, we distinguish between immediate and delayed cage exit. The former case is defined here as the cage exit probability after one vibrational period, *i.e.* 15 fs for HCl. The latter is determined as the probability of cage exit after 10 periods.

Fig. 3 shows our results for rotationally mediated photodissociation of HCl($^1\Pi$) in Ar. The initial radial wavefunction is that of the vibrational ground state $v = 0$ of the $^1\Sigma$ potential, throughout. First, it can be seen that there is a considerable probability for immediate cage exit within the first 15 fs, ranging from 0.24 to 0.57. Moreover, the short-time dynamics strongly depends on the choice of the initial rotational state. The cage-exit probability of the $J = 0$ ($A_{1g}$) and the $J = 1$ ($T_{1u}$) state are almost equal ($P = 0.42$). Although the latter is preferentially aligned along the $\langle 100 \rangle$ direction (see Fig. 1), the corresponding angular distribution is too broad to penetrate the cage formed by the nearest neighbours.

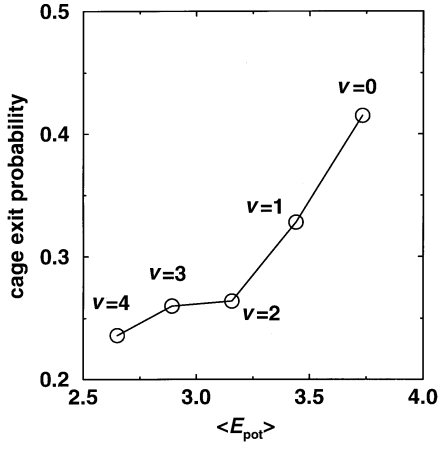


**Fig. 4** Immediate cage-exit probability $P(t = 15$ fs) of HCl in Ar (fcc) matrix as a function of the potential energy (in eV) of the initial vibrational state. In each case, the initial rotational state is $J = 0$ ($A_{1g}$).

The two sublevels of the $J = 2$ state are very different with respect to their photodissociation dynamics. While cage exit is preferred along the $\langle 100 \rangle$ direction ($E_g$) it is blocked along the $\langle 110 \rangle$ direction ($T_{2g}$). Similar results are obtained for the $J = 3$ sublevels. As could be anticipated for purely geometric reasons, the $A_{2u}$ and $T_{1u}$ states are the best candidates for immediate cage exit (0.48 and 0.57, respectively) since the lobes of the angular wavefunction point in the preferable $\langle 111 \rangle$ direction. On the contrary, chances for cage exit are lowest for the $T_{2u}$ state which is strongly pre-aligned in the $\langle 110 \rangle$ direction.

After 10 vibrational periods (150 fs) the sensitivity on the initial state geometry has decreased considerably. The probability for delayed cage exit depends only weakly on the initial rotational state and ranges only from 0.63 to 0.72. Furthermore, the order of the probabilities is partly reversed. For example, the cage exit probability of the $T_{2g}$ state is now higher than that of the $E_g$ state. This change is attributed to the coupling of the initial rotational state to higher surface harmonics of the same irreducible representation. As is apparent from the lower left corners of the radial wavefunctions in Fig. 2, the build-up of population in higher-$J$ states takes more and more time with increasing $J$. Averaging over an increasingly high number of surface harmonics then leads to a loss of selectivity.

In the following, the role of isotope effects shall be investigated. For that purpose we compare the cage-exit probability of HCl after 15 fs with that of DCl after $\sqrt{2} \times 15$ fs = 21.2 fs, in order to compensate for the different timescales. It is found that $P(t)$ increases slightly from 0.415 to 0.434 upon deuteriation. By comparing the results of two propagations, starting with exactly the same initial wavefunction but with the masses of the different isotopes, the influence of tunnelling could be ruled out. Additionally, the tiny difference in the angular part of initial state does not play a role. Hence, the 5% increase in the cage-exit probability can be attributed completely to the different radial wavefunctions of HCl and DCl. Because the vibrationally averaged bond length of DCl is slightly smaller, it gains *ca.* 3% more potential energy in a vertical transition to the repulsive $^1\Pi$ state, which facilitates immediate cage exit. On longer timescales, the difference in the photodissociation yield tends to become even smaller. After 10 vibrational periods (150 fs for HCl or 212 fs for DCl) there is no longer any isotope selectivity.

The dependence of the immediate cage-exit probability $P(t = 15$ fs) on the initial vibrational state is shown in Fig. 4 for the system HCl in Ar. For an identical initial rotational state $J = 0$ ($A_{1g}$) the probability is plotted *vs.* the expectation value $\langle E_{pot} \rangle$ of the potential energy of the initial wavefunction in the electronically excited $^1\Pi$ state. With increasing vibrational quantum number $v$ the cage exit probability decreases from 0.415 for $v = 0$ to 0.236 for $v = 4$. Again, this change in the efficiency of permanent bond breaking is a consequence of the radial wavefunction. Because both the expectation value $\langle r \rangle$ and its uncertainty increase with $v$, the averaged potential energy $\langle E_{pot} \rangle$ decreases, making an immediate cage exit less likely.

## 3 Vibrationally mediated photochemistry at surfaces

### A Desorption induced by electronic transitions (DIET) for ammonia/copper

We now consider the UV-laser-induced desorption of neutral molecules from metal surfaces. In particular, we focus on ammonia desorbing from a Cu(111) substrate.

As in the previous section the 'reaction' of interest is the cleavage of a bond by electronic excitation; in this case a molecule–surface bond. In further analogy, we vibrationally prepare the reactants to control the reaction. Isotope effects

will also be studied by replacing $NH_3$ with $ND_3$, similar to the replacement of HCl by DCl discussed above. Effects of rotational excitations are not considered in this section.

The differences to the process considered in Section 2, however, are marked. Now the condensed-phase environment surrounding the reacting 'system' not merely modifies the potentials, but has an active influence on the (electronic) dynamics of the system. Namely, electronically excited adsorbate states at metal surfaces are known to be ultra-shortlived owing to electronic quenching.[41] The quenching arises from the creation of electron–hole pairs in the metal, and the dissipation of electronic energy originally deposited in the adsorbate–substrate complex can be as fast as a few fs. The electronically excited adsorbates will also relax by coupling to phonons. The same mechanism leads to the vibrational relaxation of vibrationally excited adsorbates. Phonon-caused dissipation, however, proceeds on a much longer timescale (typically ns to μs[42]) and will, therefore, be neglected, as in the previous section.† The electronic relaxation, however, cannot be neglected and is included in the following by virtue of quantum open system density matrix theory.

DIET by UV–VIS laser light is the surface analogue to gas-phase photodissociation.[43] There are two major differences, however. First, in the gas phase the electronic excitation proceeds directly, *i.e.* by a dipole-allowed transition. In contrast, for photodesorption, if the substrate is a metal, the excitation can also be indirect, *i.e.* for example, by resonant tunnelling of 'hot', laser-excited metal electrons through a barrier separating the substrate from the adsorbate. Second, photodissociation in the gas phase usually proceeds *via* the excited state, because spontaneous emission is much slower than the bond-breaking process itself. In contrast, molecules photodesorbing from a metal are usually in their electronic ground state, because quenching is so efficient. Since the ground state is usually bound this also implies that desorption yields can be quite small; for ammonia/Cu(111), for example, only approximately 1 molecule desorbs per 1000 photons absorbed.[44,45]

DIET is frequently described by one-dimensional models, with the molecule–surface bond being the only degree of freedom considered. Further, often only the electronic ground state and a single excited state are taken into account. In the Menzel–Gomer–Redhead (MGR) model of DIET,[46] the relevant excited state is repulsive; in the so-called Antoniewicz model,[47] it is bound. The latter situation is believed to arise for NO/Pt(111), for example, where the decisive excited state is a metal-to-ligand charge transfer state, stabilized by image charge attraction.[41] In both the original MGR and the Antoniewicz models the dynamics are treated classically, and the electronic quenching introduced in an *ad hoc* fashion.

A wavepacket theory of the Antoniewicz DIET model[47] has been proposed by Gadzuk.[41] In his approach, an initial wavefunction $\Phi$ is Franck–Condon excited from the electronic ground-state surface $V_g$ to an excited potential curve, $V_e$, where it time-evolves for a certain ultrashort residence time $\tau_R$. An inverse Franck–Condon transition then takes place and the wavepacket is propagated on the ground-state surface $V_g$ up to a final time, $t_\infty$. Mathematically, this single quantum trajectory is (for $t > \tau_R$)

$$\psi(Z, t;\tau_R) = \exp\left[-\frac{i}{\hbar}\hat{H}_g(t-\tau_R)\right]\exp\left(-\frac{i}{\hbar}\hat{H}_e\tau_R\right)\Phi(Z) \quad (7)$$

where $\hat{H}_e$ and $\hat{H}_g$ are the excited- and ground-state Hamiltonians, respectively, and $Z$ is the distance between the molecule and the surface. To model the continuous exponential decay, with a lifetime $\tau$, of the excited-state resonance, Gadzuk suggested to average incoherently single-trajectory expectation values for any observable $\hat{A}$ of interest according to

$$\langle\hat{A}\rangle(t) = \frac{\int_0^\infty \exp(-\tau_R/\tau)\langle\psi(t;\tau_R)|\hat{A}|\psi(t;\tau_R)\rangle d\tau_R}{\int_0^\infty \exp(-\tau_R/\tau)d\tau_R} \quad (8)$$

As an alternative to this jumping wavepacket model we suggested to use open system nuclear density matrix theory to account for the ultrafast quenching during DIET.[48] Accordingly, one solves an open system Liouville–von Neumann equation of the form

$$\frac{d}{dt}\hat{\rho} = -\frac{i}{\hbar}[\hat{H}, \hat{\rho}] + \frac{d}{dt}\hat{\rho}_D \quad (9)$$

Here, $\hat{\rho} = \hat{\rho}_{gg}|g\rangle\langle g| + \hat{\rho}_{ge}|g\rangle\langle e| + \hat{\rho}_{eg}|e\rangle\langle g| + \hat{\rho}_{ee}|e\rangle\langle e|$ is the reduced two-state density matrix, $\hat{H} = \hat{H}_g|g\rangle\langle g| + \hat{H}_e|e\rangle\langle e|$ is the uncoupled system Hamiltonian and $(d/dt)\hat{\rho}_D$ describes the change in the density matrix due to dissipation. For the latter, a single-dissipative quenching-only model was adopted, and the so-called Lindblad form[49] used. Further, the initial state in the DIET model was the Franck–Condon transferred ground-state density, *i.e.* $\hat{\rho} = |\Phi\rangle\langle\Phi| \otimes |e\rangle\langle e|$. It can be shown[50] that this density matrix approach is rigorously equivalent to the Gadzuk wavepacket plus averaging scheme, provided that the excited state decays with a coordinate-independent quenching rate

$$\Gamma_{ge} = \tau^{-1} \quad (10)$$

In the following, we will apply Gadzuk's approach to DIET of ammonia from Cu(111). Related work has been published elsewhere.[51–56]

From the experimental point of view, this system is special because pronounced isotope effects are observed when $NH_3$ is replaced by $ND_3$. For instance, the ratio in the total desorption yields is $P_{des}(NH_3)/P_{des}(ND_3) \approx 4.1$.[44] A similarly large isotope effect was earlier found for ammonia/GaAs[57] and for ammonia/Pt(111).[56] For ammonia/Cu(111) the desorbates have also been detected in a state-resolved manner.[45,53] Here, pronounced isotope and quantum effects were seen to affect the populations of individual states of the inversion mode, $\nu_2$, of the free molecule. $NH_3$ desorbs with approximately twice the vibrational energy of $ND_3$ (and both isotopomers desorb vibrationally 'hot' when compared to the experimental surface temperature) and prefers states of *gerade* symmetry; in contrast, $ND_3$ populates *ungerade* states with higher probability.[53]

It has been, early on, realized that one-dimensional models cannot account for the isotope effects in the desorption yields of ammonia desorbing from various substrates. Zhu *et al.* have argued that at least a second internal adsorbate mode has to be taken into account.[57] Burns *et al.*[56] and Hertel *et al.*[44] identified this second mode as the inversion mode, $\nu_2$, of the ammonia molecule, which may well be idealized by the distance, $x$, of the $H_3(D_3)$ plane (which is assumed to be parallel to the surface plane) to the nitrogen atom. We define $x > 0$ if ammonia is oriented with N towards the surface, and $x < 0$ if the $H_3(D_3)$ base of the ammonia triangular pyramid is closer to the substrate.

In extension of the classical bimodal two-state model of Hertel *et al.*[44] we adopt Gadzuk's jumping wave packet plus incoherent averaging scheme for ammonia/Cu(111), using Hamiltonians of the form[52–55]

$$\hat{H}_\alpha(Z, x) = -\frac{\hbar^2}{2M}\frac{\partial^2}{\partial Z^2} - \frac{\hbar^2}{2\mu}\frac{\partial^2}{\partial x^2} + V_\alpha(Z, x); \quad (\alpha = g, e) \quad (11)$$

† Vibrationally excited adsorbates can also relax by coupling to the electron–hole pair continuum of a metal. This process can occur on a ps timescale, but will also be neglected here.

where $Z$ is the distance of the molecule's centre of mass from the surface, $x$ the idealized inversion mode and $M$ and $\mu$ are the corresponding reduced masses. For the ground and excited states $V_g$ and $V_e$ model potentials are used.[44,51] The ground state gives the familiar symmetric double-well potential of the free ammonia inversion mode when the limit $Z \rightarrow \infty$ is taken; closer to the surface, the inversion symmetry is broken and a chemisorption well for $x > 0$ arises (binding energy *ca.* 5600 $cm^{-1}$) and simultaneously a less pronounced well for the inverted adsorbate ($x < 0$; binding energy *ca.* 2800 $cm^{-1}$).[51] The excited state, $V_e$, is assumed to be situated several eV above $V_g$, and to be harmonic in both coordinates; the excited state equilibrium structure is a flat ammonia molecule, with a distance to the surface of *ca.* 4 $a_0$.

In the following, isotope effects will be derived by employing different initial states $\Phi$ in eqn. (7). These initial states are vibrational bound states for the electronic ground-state surface $V_g$, and may selectively be populated by IR laser pulses, for example. Hence, in the following, an IR plus UV experiment is to be modelled with the aim to achieve selective photochemistry at metal surfaces.

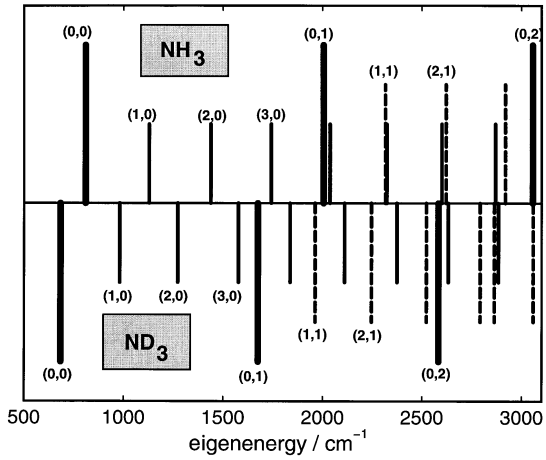


**Fig. 5** Schematic representation of the eigenenergies $\varepsilon_g^n$ of $NH_3$ and $ND_3$ molecules adsorbed on a Cu model surface. For selected states, nodal labels ($n_z$, $n_x$) are attached. The thin, short and solid sticks show the progression of states which are excited in the molecule–surface bond only. The thick, long, solid sticks show the progression of states which are excited in the umbrella mode only. The dashed sticks denote combination modes. The energies are measured relative to the bottom of the 'canonical' chemisorption well.

### B State-selective vibrational preparation step

The initial states $\Phi$ adopted below are eigenfunctions of the ground-state Hamiltonian $\hat{H}_g$ defined in eqn. (11), *i.e.* $\Phi = |n_g\rangle$ and

$$\hat{H}_g |n_g\rangle = \varepsilon_g^n |n_g\rangle \tag{12}$$

Eqn. (12) has been solved along the lines described elsewhere.[51] The eigenfunctions $\{|n_g\rangle\}$ can, for energies not too large, be classified according to their numbers of nodes in the 'umbrella' mode $x$, and in the molecule–surface mode $Z$:

$$|n_g\rangle \coloneqq |n_z, n_x\rangle \tag{13}$$

The molecule–surface bond is 'soft' (the $NH_3$ excitation energy for the transition $|1, 0\rangle \leftarrow |0, 0\rangle$ is 319 $cm^{-1}$), while the inversion mode is 'stiff' (the $NH_3$ excitation for the transition $|0, 1\rangle \leftarrow |0, 0\rangle$ is 1195 $cm^{-1}$). (Both values agree well with experimental vibrational frequencies.[58]) Hence, for the adsorbate–surface complex a van der Waals-type situation arises, with the umbrella-mode excited states being energetically well separated from each other, and embedded in the denser background spectrum of the molecule–surface progression. This situation is shown schematically in Fig. 5, giving the computed vibrational state energies for $NH_3$ and $ND_3$ together with their nodal classification, up to an energy of approximately 3000 $cm^{-1}$ above the bottom of the 'canonical' chemisorption well are shown.

From the figure, we also note that the molecule–surface fundamental frequencies are very similar for $NH_3$ and $ND_3$ (319 *cf.* 297 $cm^{-1}$; in contrast, excitation into the inversion mode is substantially different (1195 *cf.* 991 $cm^{-1}$). This is due to the similarity of the adsorbate masses [$M(NH_3)/M(ND_3) \approx 0.85$], and the dissimilarity of the reduced masses for inversion [$\mu(NH_3)/\mu(ND_3) \approx 0.59$]. The substantially different resonance frequencies for the inversion modes will be the basis for the isotope-selective DIET experiment proposed below.

The DIET experiments performed so far were carried out at low surface temperatures ($T_s \approx 120$ K), and hence started out from the vibrational ground state $|0, 0\rangle$. We may also consider using vibrationally excited initial states, selectively populated by an IR laser pulse in the ps domain. The theoretical modelling of such a vibrational preparation step requires the explicit inclusion of the IR laser field $E(t)$ (we consider the $z$-component of the field only), and knowledge of the dipole transition matrix elements connecting final with initial vibrational ground states, *i.e.*

$$\mu_{gg}^{fi} \coloneqq \langle f_g | \mu_{gg}(Z, x) | i_g \rangle \tag{14}$$

Here, $\mu_{gg}(Z, x)$ is the $z$-component of the electronic ground-state dipole function, and the integration in eqn. (14) is done over the nuclear coordinates. Based on simple *ab initio* cluster calculations we have recently devised a model form for $\mu_{gg}(Z, x)$.[54] This dipole function is asymptotically proportional to $x$,

$$\lim_{Z \rightarrow \infty} \mu_{gg}(Z, x) \propto x \tag{15}$$

and is slightly more complicated closer to the surface.

In Table 2, we give certain selected transition dipole moments squared, $|\mu_{gg}^{fi}|^2$ for both isotopomers, as computed from the model dipole function of ref. 54 and the ground-state eigenfunctions $|n_g\rangle$.

It is immediately clear that excitation of the umbrella-excited states should be a much easier task than preparation of only molecule–surface excited final states. This is due to the approximate form (15) of the dipole function, making the matrix elements for the excitation of the inversion mode orders of magnitude larger than those for molecule–surface transitions. Further, the doubly inversion excited state $|0, 2\rangle$ may be populated by a two-photon strategy *via* the first excited state; this is to be anticipated from the large matrix elements for the $|0, 1\rangle \leftarrow |0, 0\rangle$ and $|0, 2\rangle \leftarrow |0, 1\rangle$ transitions.

**Table 2** Selected transition dipole moments squared, $|\mu_{gg}^{fi}|^2$ connecting initial states $|i_g\rangle = |i_z, i_x\rangle$ with final $|f_g\rangle = |f_z, f_x\rangle$ ones for $NH_3$ and $ND_3$ adsorbed on a model Cu surface, the transition frequencies are also given

| final state $\|f_g\rangle$ | initial state $\|i_g\rangle$ | $\|\mu_{gg}^{fi}\|^2$/a.u. | | $(\varepsilon_g^f - \varepsilon_g^i)/cm^{-1}$ | |
|---|---|---|---|---|---|
| | | $NH_3$ | $ND_3$ | $NH_3$ | $ND_3$ |
| $\|1, 0\rangle$ | $\|0, 0\rangle$ | $2.3 \times 10^{-5}$ | $1.4 \times 10^{-4}$ | 319 | 297 |
| $\|2, 0\rangle$ | $\|0, 0\rangle$ | $9.1 \times 10^{-5}$ | $1.4 \times 10^{-4}$ | 629 | 587 |
| $\|3, 0\rangle$ | $\|0, 0\rangle$ | $3.0 \times 10^{-6}$ | $8.7 \times 10^{-6}$ | 931 | 872 |
| $\|0, 1\rangle$ | $\|0, 0\rangle$ | $2.5 \times 10^{-2}$ | $1.8 \times 10^{-2}$ | 1195 | 991 |
| $\|0, 2\rangle$ | $\|0, 0\rangle$ | $4.1 \times 10^{-4}$ | $2.5 \times 10^{-4}$ | 2248 | 1898 |
| $\|0, 2\rangle$ | $\|0, 1\rangle$ | $5.4 \times 10^{-2}$ | $3.8 \times 10^{-2}$ | 1053 | 908 |

These expectations are confirmed by simulations, in which the semi-classical dipole approximation for the molecule–field coupling, and sequences of IR pulses of $\sin^2$ form have been used and optimized to achieve maximum populations for selected target states.[54] Neglecting vibrational relaxation, almost complete (>90%) population transfer to both lowest umbrella-excited states $|0, 1\rangle$ and $|0, 2\rangle$ can be obtained using one- or two-pulse IR fields of finite spectral width. (Both 0.5 and 1.0 ps pulses proved successful.) In contrast, the significant excitation of the lowest molecule–surface excited states is impossible with realistic lasers. The extreme bond selectivity encountered for the IR preparation step is a consequence of the substantially different matrix elements listed in Table 2.

Importantly, it also observed that the isotope-selective preparation of either the $NH_3$ or the $ND_3$ umbrella mode is possible. Applying, for example, the IR pulse sequence proven optimal for the selective population of the $NH_3$ $|0, 2\rangle$ state, to coadsorbed $ND_3$, does not lead to any $ND_3$ final state populations larger than $0.2 \times 10^{-3}$. This isotope-selective state preparation by finite-width lasers is a consequence of the bond selectivity on the one hand, and the substantially different umbrella frequencies on the other.

### C The DIET step

The indirect, UV-cw laser-induced DIET of ammonia from Cu(111) using various initial states $\Phi = |n_z, n_x\rangle$ is modelled along the lines drawn in Section 3A. Because, obviously, only those excited vibrational states can seriously be considered which have at least one node in their umbrella mode, we restrict to $\Phi = |0, 0\rangle$, $\Phi = |0, 1\rangle$ and $\Phi = |0, 2\rangle$ in the following. Since vibrational relaxation is neglected, the exact moment of the electronic Franck–Condon transition is unimportant and is defined as the time zero in eqn. (7). The inclusion of vibrational relaxation is the subject of a forthcoming investigation.[59]

Numerical details describing the wavepacket propagation required to solve eqn. (7) and to evaluate eqn. (8) can be found elsewhere.[52,55] In short, we represent the wavefunctions on a grid and employ fast Fourier transform to evaluate the kinetic-energy operator locally. The split-operator propagator of Feit and Fleck[60] is used to factorize further the exponentials in eqn. (7). The total propagation time $t_\infty = 1$ ps. The incoherent averaging, eqn. (8), is done at 100 sampling points $\tau_R$ in the interval between 0.25 and 25 fs. We compute (1) total unaveraged and averaged desorption probabilities, $P_{des}(\tau_R)$ and $\langle P_{des}\rangle$, respectively, (2) (umbrella-)vibrational energies $\langle E_{vib}\rangle$ for the desorbates and (3) desorbate kinetic energies $\langle E_{trans}\rangle$. We also define isotope effects for the product yield, the desorbate vibrational energy and the desorbate translational energy as

$$R_{des} := \frac{\langle P_{des}\rangle(NH_3)}{\langle P_{des}\rangle(ND_3)} \quad (16)$$

$$R_{vib} := \frac{\langle E_{vib}\rangle(NH_3)}{\langle E_{vib}\rangle(ND_3)} \quad (17)$$

$$R_{trans} := \frac{\langle E_{trans}\rangle(NH_3)}{\langle E_{trans}\rangle(ND_3)} \quad (18)$$

In a first step, the, so far unknown, excited state lifetime $\tau$ occurring in eqn. (8) is determined semi-phenomenologically by comparing the computed isotope effect in the yields, $R_{des}$, with the experimental value of $R_{des} \approx 4.1$.[44] To model the experiment, $\Phi = |0, 0\rangle$ is used.

The isotope effect $R_{des}$, computed for various lifetimes $\tau$ is found to rapidly decrease with $\tau$ increasing [see Fig. 6(a)]. Best agreement with the experimental value is obtained for the ultrashort resonance lifetime $\tau = 1.5$ fs.‡ This isotope effect is due to the fact that the heavier isotopomer accelerates less efficiently on the excited-state potential towards planarization and, hence, reaches only less repulsive regions of the ground-state potential after de-excitation. As a consequence, the probability to desorb on $V_g$ is larger for $NH_3$ than for $ND_3$. In the present formalism, the averaged desorption probability arises from integration over weighted, unaveraged probabilities $P_{des}(\tau_R)\exp(-\tau_R/\tau)$ in eqn. (8). In Fig. 7(a), the integrand to eqn. (8) is shown for both isotopomers, and $\tau = 1.5$ fs and $\Phi = |0, 0\rangle$. It is seen that despite the lifetime $\tau$ being so short, the actual quantum trajectories which lead to desorption are those with a residence time around $\tau_R \approx 7$ fs, where the integrand has its maximum. The computed averaged desorption probabilities $\langle P_{des}\rangle(NH_3)$ and $\langle P_{des}\rangle(ND_3)$ are $3.05 \times 10^{-3}$ and $7.20 \times 10^{-4}$, respectively and, therefore, in good agreement with experiment.[44,45]

In further agreement with experiment we find that the molecules desorb highly excited in their $\nu_2$-mode. While the absolute values are somewhat too high in theory (because the model is only two-dimensional), the experimental vibrational isotope effect is well accounted for [$R_{vib}^{the}(\tau = 1.5$ fs$) = 1.75$, $R_{vib}^{exp} = 1.64$]. The vibrational isotope effect can be rationalized by assuming that the desorbates follow, quasi-adiabatically, a curved reaction path on the ground state, as argued in more detail in ref. 46.

From Fig. 6(a), where the vibrational isotope effect is shown as a function of $\tau$, we note that $R_{vib}$ does not depend so much on $\tau$ as $R_{des}$ does. This is due to the fact that the absolute values of $\langle E_{vib}\rangle$ increase only moderately between $\tau = 1$ and 5 fs (the variation is no more than a factor of 2), while the desorption yields increase almost exponentially with increas-

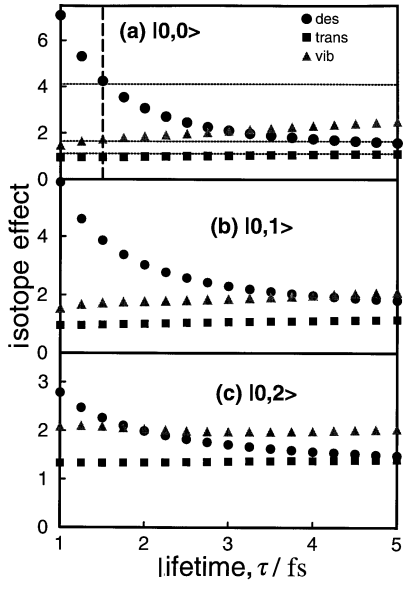


**Fig. 6** Computed isotope effects in the desorption yields ($R_{des}$, ●), the (umbrella-)vibrational desorbate energy ($R_{vib}$, ■) and the translational desorbate energy ($R_{trans}$, ▲) for both adsorbed $NH_3$ and $ND_3$ as a function of the resonance lifetime $\tau$. As DIET initial states, the vibrational ground states [(a), $|0, 0\rangle$], the first inversion mode excited states [(b), $|0, 1\rangle$] and the second inversion mode excited states [(c), $|0, 2\rangle$], have been used. In (a), additionally the experimental values are given as dashed horizontal lines ($R_{des}^{exp} = 4.1$, $R_{vib}^{exp} = 1.64$, $R_{trans}^{exp} = 1.1$). Note that for $\tau = 1.5$ fs (dashed vertical line), good agreement with all measured isotope effects is simultaneously obtained.

‡ In ref. 52 and 53, slightly shorter and longer lifetimes, respectively, were estimated. This was due to a shorter propagation time, a smaller grid and less residence times $\tau_R$ than used here.

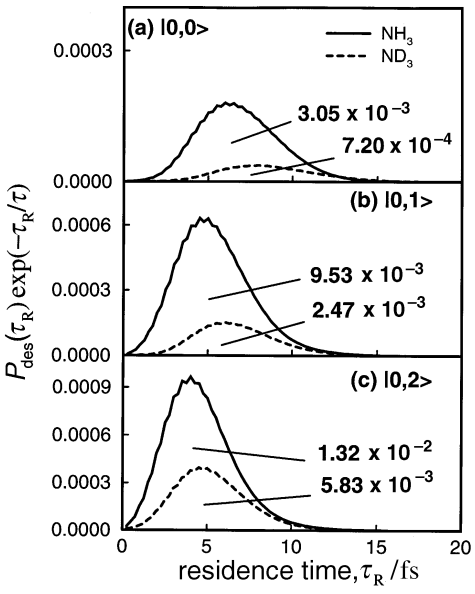


**Fig. 7** Integrands $P_{des}(\tau_R)\exp(-\tau_R/\tau)$ for both isotopomers, the initial states (a)–(c) of Fig. 6, and for a resonance lifetime of $\tau = 1.5$ fs, as a function of the residence time, $\tau_R$. The areas under the curves are proportional to the (averaged) desorption yields $\langle P_{des}\rangle$. The computed averaged desorption yields are the numbers attached to each curve.

ing $\tau$. (For $NH_3$, the yield increases by a factor of *ca.* 100, for $ND_3$ by a factor of *ca.* 350.)

The translational isotope effect $R_{trans}$ also varies only weakly with $\tau$, and is always *ca.* 1. The measured value is 1.1.[45,54] The desorbates are translationally more excited than the corresponding surface temperature might suggest, but not to the same degree as found for vibration. This is also in good agreement with experiment,[45,46] as is the absence of correlations between translation and vibration. (The state-resolved translational energies are all very similar.)

Hence, reasonable agreement between theory and experiment can be obtained simply by adjusting the lifetime $\tau$ to reproduce the isotope effect in the total yields. All other theoretical quantities follow without further adjustment. This procedure not only gives the (ultrashort) order of magnitude for the lifetime, but also predicts the dependence of certain observables on $\tau$. $\tau$ Is therefore a control parameter for the active manipulation of product-branching ratios, for example. Control of $\tau$ may be achieved, in principle, by separating the adsorbate and the substrate by rare-gas spacers.

A more promising control strategy is vibrationally mediated chemistry, as anticipated above. In Fig. 6(b) and 7(b) the analogous information to Fig. 6(a) and 7(a) is given; the only difference being that now the initial states $\Phi = |0, 1\rangle$ have been used for both isotopomers. From Fig. 6(b) it is seen that the averaged desorption yield increases substantially, by factors of 3.1 ($NH_3$) and 3.4 ($ND_3$), respectively. Note that the enhanced reactivity, despite ultrafast electronic quenching, is operative. (For unaveraged desorption yields $P_{des}(\tau_R = 1.5$ fs), factors of 6.3 ($NH_3$) and 19.2 ($ND_3$) are obtained.) Hence, laser control in the condensed phase seems still possible, but is not as effective as in the gas phase.

From Fig. 6(b) it is seen that the isotope effects as a function of $\tau$ behave qualitatively similarly to the $\Phi = |0, 0\rangle$ case. Quantitatively, we find, in particular, that the isotope effect for the yields, $R_{des}$, does not fall off as rapidly as without vibrational preparation [Fig. 6(a)]. This is due to the more 'smoothed out' $P_{des}(\tau_R)$ curves characteristic for $\Phi = |0, 1\rangle$.

Finally, we show results for the $\Phi = |0, 2\rangle$ initial state case [see Fig. 6(c) and 7(c)]. A further increase of the averaged desorption probabilities is achieved (by a factor of 4.3 ($NH_3$) and 8.1 ($ND_3$), respectively, at $\tau = 1.5$ fs). Since the yield increases more for the heavier isotopomer, the isotope effect becomes substantially smaller than previously. At $\tau = 1.5$ fs, it is close to the predicted vibrational isotope effect, $R_{vib}$. The latter increases substantially with $\tau$, while the translational isotope effect, $R_{trans}$, is again almost unaffected.

The isotope effects given so far were computed by assuming that both the $NH_3$ and $ND_3$ DIET initial states have the same nodal structure. As argued in Section 3B, however, an IR pulse sequence optimal for excitation of the $NH_3$ umbrella mode, say, will not affect the (vibrational ground state) population of coadsorbed $ND_3$ and *vice versa.* Hence, in an IR–UV DIET experiment where both isotopomers are simultaneously adsorbed on the substrate, one better considers isotope effects of the form

$$R_{des} = \frac{\langle P_{des}\rangle(NH_3;\, \Phi_1)}{\langle P_{des}\rangle(ND_3;\, \Phi_2)} \tag{19}$$

Here, $\Phi_1$ is $|0, 0\rangle$ when $\Phi_2$ is an umbrella-excited $ND_3$ state and $\Phi_2$ is $|0, 0\rangle$ when $NH_3$ was IR-prepared. In Table 3, the (averaged) isotope effect, eqn. (19), is given for various $\Phi_1/\Phi_2$ combinations and $\tau = 1.5$ fs. It is seen that, in this case, a control of the isotope effect by IR vibrational excitation of the adsorbate is possible. From the relative $NH_3$ desorption yields, which are also given, it is seen that $NH_3$ can be desorbed almost selectively (when $NH_3$ was doubly excited), or that predominantly $ND_3$ products can be obtained (when $ND_3$ was doubly excited). Again, this isotope-selective photodesorption is achieved in the presence of very strong dissipation.

It is also demonstrated in Table 3, for the hypothetical $\tau = 1$ fs case, that selectivity may be more pronounced in systems where the lifetimes are small and, therefore, the desorption yields are low. In this case, dissipation is even stronger but huge isotope effects, and variations of them, can be achieved. Extremely large isotope effects (of the order of 50) in low-yield DIET systems, have been observed experimentally for the (scanning tunnelling microscope-induced) desorption of H or D from stepped Si surfaces, for example.[61]

We close this section by noting that the IR–UV DIET experiment proposed here is conceptually similar to an IR + UV pump–UV dump three-pulse experiment, which has been suggested for the cleavage of gas-phase molecules.[16] In the present example, however, the electronic 'dump' step is replaced by the naturally occurring electronic quenching. Further, the IR laser prepares not the bond to be broken, but rather an internal ammonia mode. This is in perfect line with the initial motion of ammonia along the $\nu_2$ mode after electronic excitation, which is assumed to be a key property for this and similar desorption systems.[44,51,56,57]

**Table 3** Isotope-selective photodesorption for the ammonia/Cu system

| $\phi_1$ | $\phi_2$ | $\langle P_{des}(NH_3)\rangle$ | $\langle P_{des}(ND_3)\rangle$ | $R_{des}$ | yield $NH_3$ (%) |
|---|---|---|---|---|---|
| $\tau = 1.5$ fs | | | | | |
| $\|0, 0\rangle$ | $\|0, 0\rangle$ | $3.05 \times 10^{-3}$ | $7.20 \times 10^{-4}$ | 4.24 | 81 |
| $\|0, 1\rangle$ | $\|0, 0\rangle$ | $8.99 \times 10^{-3}$ | $7.20 \times 10^{-4}$ | 12.49 | 93 |
| $\|0, 2\rangle$ | $\|0, 0\rangle$ | $1.32 \times 10^{-2}$ | $7.20 \times 10^{-4}$ | 18.33 | 95 |
| $\|0, 0\rangle$ | $\|0, 1\rangle$ | $3.05 \times 10^{-3}$ | $2.47 \times 10^{-3}$ | 1.23 | 55 |
| $\|0, 0\rangle$ | $\|0, 2\rangle$ | $3.05 \times 10^{-3}$ | $5.83 \times 10^{-3}$ | 0.52 | 34 |
| $\tau = 1.0$ fs | | | | | |
| $\|0, 0\rangle$ | $\|0, 0\rangle$ | $6.47 \times 10^{-4}$ | $9.13 \times 10^{-5}$ | 7.09 | 88 |
| $\|0, 1\rangle$ | $\|0, 0\rangle$ | $3.12 \times 10^{-3}$ | $9.13 \times 10^{-5}$ | 34.17 | 97 |
| $\|0, 2\rangle$ | $\|0, 0\rangle$ | $5.41 \times 10^{-3}$ | $9.13 \times 10^{-5}$ | 59.26 | 98 |
| $\|0, 0\rangle$ | $\|0, 1\rangle$ | $6.47 \times 10^{-4}$ | $5.34 \times 10^{-4}$ | 1.21 | 55 |
| $\|0, 0\rangle$ | $\|0, 2\rangle$ | $6.47 \times 10^{-4}$ | $1.94 \times 10^{-3}$ | 0.33 | 25 |

Given are the averaged desorption probabilities $\langle P_{des}\rangle$ for $NH_3$ and $ND_3$, the isotope effect in the yields, $R_{des}$, and the relative yield of $NH_3$. This is done for different DIET initial state combinations $\Phi_1(NH_3)$ and $\Phi_2(ND_3)$; the $\tau = 1.5$ fs and the hypothetical $\tau = 1$ fs cases are considered.

## 4 Conclusions

We have investigated two extensions of the concept of vibrationally mediated chemistry, from small molecules in the gas phase to small molecules in matrices and at surfaces. Both systems and processes studied, HCl in Ar and ammonia at copper have, in common, the photo-induced breaking of a molecular bond in a condensed-phase environment. In the first case, photodissociation of matrix isolated molecules is considered, in the second case, the photodesorption of an adsorbate from a surface is of interest. In either case, the reactants were prepared by IR-induced (ro-vibrational) excitation. The step from isolated systems to the condensed phase calls for corresponding extensions of the methods and allows the discovery of new quantum dynamical aspects. In Section 2 the photodissociation of HCl in an Ar matrix is treated by fully dimensional quantum mechanical wavepacket propagation for the light photofragment. This allows an investigation of the role of the initial ro-vibrational state in photodissociation dynamics of matrix-isolated molecules. It has been shown that vibrational excitation substantially lowers the immediate cage-exit probability by reducing the excess energy. This mechanism could be used in future experiments to determine the energetic threshold for direct cage exit. The concept of vibrationally mediated photodissociation has been extended here to include rotational states. As a consequence of the external field, the rotational states favour certain crystallographic orientations which give rise to different cage exit probabilities. However, this concept of ro-vibrationally mediated chemistry is limited to the domain of very short times, comparable to one oscillation period of the rattling vibration of the light photofragment. This time resolution can be achieved in state-of-the-art pump–probe experiments. On larger timescales, this type of selectivity is reduced by matrix effects.

For the photodesorption of ammonia from copper, reasonable agreement between theory and existing experiments has been obtained with a comparatively simple dissipative two-state model. We have also seen that bond, and isotope, selective chemistry seems possible for this system, although electronic quenching is present and occurs on a fs timescale. The electronic relaxation has been utilized as a naturally occuring 'dump' step within the proposed preparation–excitation–de-excitation control strategy. In this way, vibrational preparation with IR laser pulses was shown to allow for the control of isotope effects over a wide range. Ultimately, the corresponding extension of the traditional DIET process to the IR–UV DIET scheme suggested here should yield selective enrichment of isotopomers at surfaces, *e.g.* $ND_3$, not $NH_3$ at Cu(111).

Irrespective of the new phenomena we emphasize, however, that the present investigations should provide nothing but a first step from the 'classic' domain of vibrationally mediated chemistry in gases to the new regime of the condensed phase. The corresponding new methods of quantum dynamics are, in fact, tailored to these new phenomena, but they involve many approximations which should be replaced by more rigorous approaches beyond the present paper.

For the simulation of photodissociation of HCl in Ar there are two principle limitations of the model used here. (1) The first simplifying assumption is the neglect of recombination. Transitions from the $^1\Pi$ state back to the $^1\Sigma$ ground state were investigated in ref. 24 and 25. It could be shown, by means of classical trajectories including surface hopping, that recombination has a quantum yield of the order of 50%. Including this effect in our simulation would certainly lead to lower cage-exit probabilities than predicted here. On the other hand, it would not affect the possibility of ro-vibrationally mediated chemistry. (2) Another limitation of our model is the rigidity of the rare-gas cage. The process of indirect cage exit, where the H-atom photofragment locally distorts the matrix in the course of one or more rattling vibrations, has not been treated here. One effect of a flexible cage is the energy loss of the light fragment in collisions with the cage atoms. The higher energy loss of D as compared to H leads to a much lower photodissociation quantum yield, which has been observed experimentally for $H_2O$ and $H_2S$[21] in rare-gas matrices. By neglecting the flexibility of the matrix atoms, this isotope effect has not been observed in our simulations. Here, only an inverse (but much weaker) isotope effect has been found, which is due to the different bond length of HCl and DCl. One way to incorporate indirect cage exit would be a quantum–classical hybrid treatment, where only the H atom is treated quantum mechanically while the remaining particles are modelled as classical point masses. This kind of hybrid mechanics has been realized in simulations of HI in a Xe matrix[26] and $I_2$ in a linear Ar chain.[27] Similar work is in progress for the system considered here.[32]

For the ammonia/copper system the inclusion of vibrational relaxation, which opposes selective vibrational excitation, is the most urgent task. Further, the use of ps UV lasers [rather than ns (cw) lasers as modelled, here] might have interesting effects. In this case, the so-called DIMET (desorption induced by multiple electronic transitions) limit is reached,[62] and significantly different isotope effects may be observed.

Finally, it should be mentioned that, in the simulations of both the photodissociation in matrices and of surface photodesorption, the process of UV excitation is realized by a vertical transition of the wavepacket which is equivalent to excitation with a $\delta$-shaped laser pulse. In order to calculate the dissociation/desorption efficiency with a cw laser, projection techniques would have to be applied, see *e.g.* ref. 63. Another aspect to be investigated is vibrationally or ro-vibrationally mediated chemistry in the condensed phase for different IR–UV photon energies.

As a further illustration of the wavepacket dynamics such as shown in Fig. 2 we recommend viewing our MPEG movies on the World Wide Web at location http://www.chemie.fu-berlin.de/manz/

Financial support by the DFG through SFB 337 "Energie- und Ladungs transfer in molekularen Aggregaten" and through project no. Sa 574/2-1 as well as by Fonds der Chemischen Industrie is acknowledged. We would like to thank J. M. Hutson and M. Lewerenz for providing us with parts of the computer codes, and G. K. Paramonov for fruitful discussions.

### References

1 V. S. Letokhov, *Science*, 1973, **180**, 451.
2 P. F. Zittel and D. D. Little, *J. Chem. Phys.*, 1979, **71**, 713.
3 F. F. Crim, *Science*, 1990, **249**, 1387.
4 R. L. Van der Wal, J. L. Scott and F. F. Crim, *J. Chem. Phys.*, 1990, **92**, 803.
5 S. S. Brown, H. L. Berghout, R. B. Metz and F. F. Crim, *J. Chem. Phys.*, in the press.
6 F. F. Crim, *Annu. Rev. Phys. Chem.*, 1993, **44**, 397.
7 F. F. Crim, *J. Phys. Chem.*, 1996, **100**, 12725.
8 A. Sinha, M. C. Hsiao and F. F. Crim, *J. Chem. Phys.*, 1991, **94**, 4928.
9 M. Shapiro and E. Segev, *J. Chem. Phys.*, 1982, **77**, 5604.
10 V. Engel and R. Schinke, *J. Chem. Phys.*, 1988, **88**, 6831; V. Engel, R. Schinke and V. Staemmler, *J. Chem. Phys.*, 1988, **88**, 129.
11 J. Zhang and D. J. Imre, *Chem. Phys. Lett.*, 1988, **149**, 233; D. J. Imre and J. Zhang, *Chem. Phys.*, 1989, **139**, 89.
12 K. Kudla and G. C. Schatz, *J. Chem. Phys.*, 1993, **98**, 4644 and references therein.
13 D. Wang and J. M. Bowman, *J. Chem. Phys.*, 1992, **96**, 8906.
14 D. H. Zhang, *J. Chem. Phys.*, 1993, **99**, 5615.

15 J. E. Combariza, C. Daniel, B. Just, E. Kades, E. Kolba, J. Manz, W. Malisch, G. K. Paramonov and B. Warmuth, in *Isotope Effects and Gas-Phase Chemistry*, ed. J. A. Kaye, ACS Symposium Series 502, American Chemical Society, Washington, DC, 1992, p. 310.
16 C. Daniel, R. de Vivie-Riedle, M-C. Heitz, J. Manz and P. Saalfrank, *Int. J. Quant. Chem.*, 1996, **57**, 595.
17 C. Daniel, M-C. Heitz, L. Lehr, J. Manz and T. Schröder, *J. Phys. Chem.*, 1993, **97**, 12485.
18 M. Chergui and N. Schwentner, *Trends Chem. Phys.*, 1992, **2**, 89.
19 R. Alimi, R. B. Gerber and V. A. Apkarian, *J. Chem. Phys.*, 1990, **92**, 3551.
20 R. Schriever, M. Chergui, H. Kunz, V. Stepanenko and N. Schwentner, *J. Chem. Phys.*, 1989, **91**, 4128; R. Schriever, M. Chergui and N. Schwentner, *J. Chem. Phys.*, 1990, **93**, 9206; *J. Phys. Chem.*, 1991, **95**, 6124.
21 J. Zoval and V. A. Apkarian, *J. Phys. Chem.*, 1994, **98**, 7945.
22 K. H. Gödderz, N. Schwentner and M. Chergui, *J. Chem. Phys.*, 1996, **105**, 451.
23 R. Alimi, R. B. Gerber and V. A. Apkarian, *J. Chem. Phys.*, 1988, **89**, 174; R. Alimi and R. B. Gerber, *Chem. Phys. Lett.*, 1990, **173**, 393.
24 I. H. Gersonde and H. Gabriel, *J. Chem. Phys.*, 1993, **98**, 2094.
25 A. I. Krylov and R. B. Gerber, in *Ultrafast Chemical and Physical Processes in Molecular Systems*, ed. M. Chergui, World Scientific, Singapore, 1996, p. 628; A. I. Krylov and R. B. Gerber, *J. Chem. Phys.*, to be published.
26 R. Alimi and R. B. Gerber, *Phys. Rev. Lett.*, 1990, **64**, 1453; R. B. Gerber and R. Alimi, *Chem. Phys. Lett.*, 1990, **173**, 393.
27 L. Liu and H. Guo, *Chem. Phys. Lett.*, 1995, **237**, 299; *J. Chem. Phys.*, 1996, **104**, 528.
28 R. Alimi, A. Brokman and R. B. Gerber, *J. Chem. Phys.*, 1989, **91**, 1611.
29 H. Kunttu and V. A. Apkarian, *Chem. Phys. Lett.*, 1990, **171**, 4856.
30 A. V. Benderskii and C. A. Wight, *J. Chem. Phys.*, 1994, **101**, 292.
31 B. Schmidt, P. Jungwirth and R. B. Gerber, in ref. 25. p. 637.
32 B. Schmidt, *J. Chem. Phys.*, in preparation.
33 R. C. Mowrey and D. J. Kouri, *J. Chem. Phys.*, 1986, **84**, 6466.
34 C. J. Bradley and A. P. Cracknell, *The Mathematical Theory of Symmetry in Solids*, Clarendon, Oxford, 1972.
35 J. M. Hutson, *J. Phys. Chem.*, 1992, **96**, 4237.
36 D. M. Hirst and M. F. Guest, *Mol. Phys.*, 1980, **41**, 1483.
37 K. T. Tang and J. P. Toennies, *Chem. Phys.*, 1991, **156**, 413.
38 R. Kosloff, *J. Phys. Chem.*, 1988, **92**, 2087.
39 B. Schmidt and P. Jungwirth, *Chem. Phys. Lett.*, 1996, **259**, 62.
40 H. E. Hallam, in *Vibrational Spectroscopy of Trapped Species*, ed. H. E. Hallam, Wiley, London, 1973, p. 67.
41 J. W. Gadzuk and C. W. Clark, *J. Chem. Phys.*, 1989, **91**, 3174; J. W. Gadzuk, L. J. Richter, S. A. Buntin, D. S. King and R. R. Cavanagh, *Surf. Sci.*, 1990, **235**, 317; J. W. Gadzuk, *Phys. Rev. B*, 1991, **44**, 13; J. W. Gadzuk, *Surf. Sci.*, 1995, **342**, 345.
42 P. Guyot-Sionnest, P. Dumas, Y. J. Chabal and G. Higashi, *Phys. Rev. Lett.*, 1990, **64**, 2156; Y. J. Chabal, *J. Mol. Struct.*, 1993, **292**, 65.
43 See *Desorption Induced by Electronic Transitions Workshops Proceedings*, Springer, Berlin.
44 T. Hertel, M. Wolf and G. Ertl, *J. Chem. Phys.*, 1995, **102**, 3414.
45 W. Nessler, K-H. Bornscheuer, T. Hertel and E. Hasselbrink, *Chem. Phys.*, 1995, **205**, 205.
46 D. Menzel and R. Gomer, *J. Chem. Phys.*, 1964, **41**, 3311; P. A. Redhead, *Can. J. Phys.*, 1964, **42**, 886.
47 P. R. Antoniewicz, *Phys. Rev. B*, 1980, **21**, 3811.
48 P. Saalfrank, R. Baer and R. Kosloff, *Chem. Phys. Lett.*, 1994, **230**, 463; P. Saalfrank and R. Kosloff, *J. Chem. Phys.*, 1996, **105**, 2441.
49 G. Lindblad, *Commun. Math. Phys.*, 1976, **48**, 119; V. Gorini and A. Kossakowski, *J. Math. Phys.*, 1976, **17**, 821.
50 P. Saalfrank, *Chem. Phys.*, 1996, **211**, 265.
51 P. Saalfrank, S. Holloway and G. R. Darling, *J. Chem. Phys.*, 1995, **103**, 6720.
52 E. Hasselbrink, M. Wolf, S. Holloway and P. Saalfrank, *Surf. Sci.*, 1996, **363**, 179.
53 K-H. Bornscheuer, M. Binetti, W. Nessler, E. Hasselbrink and P. Saalfrank, *Phys. Rev. Lett.*, in the press.
54 G. K. Paramonov and P. Saalfrank, *J. Chem. Phys.*, submitted.
55 H. Guo, *Chem. Phys. Lett.*, 1995, **240**, 393; H. Guo and T. Seideman, *J. Chem. Phys.*, 1995, **103**, 9062.
56 A. R. Burns, D. R. Jennison, E. B. Stechel and Y. S. Li, *Phys. Rev. Lett.*, 1992, **68**, 3359; A. R. Burns, E. B. Stechel, D. R. Jennison and Y. S. Li, *J. Chem. Phys.*, 1994, **101**, 6318.
57 X-Y. Zhu and J. M. White, *Phys. Rev. Lett.*, 1992, **68**, 3359; X-Y. Zhu, M. Wolf, T. Huett and J. M. White, *J. Chem. Phys.*, 1992, **97**, 5868; X-Y. Zhu, *J. Chem. Phys.*, 1993, **98**, 3410.
58 I. Hussla and T. J. Chuang, *Ber. Bunsen-Ges. Phys. Chem.*, 1985, **89**, 294.
59 G. K. Paramonov and P. Saalfrank, in preparation.
60 M. D. Feit, J. Fleck Jr. and A. Steiger, *J. Comput. Phys.*, 1982, **47**, 412.
61 Ph. Avouris, R. E. Walkup, A. R. Rossi, H. C. Akpati, P. Nordlander, T-C. Shen, G. C. Abeln and J. W. Lyding, *Surf. Sci.*, 1996, **363**, 368.
62 J. A. Misewich, T. F. Heinz and D. M. Newns, *Phys. Rev. Lett.*, 1992, **68**, 3737.
63 G. G. Balint-Kurti, F. Göttgas, St. Mort, A. R. Offer, A. Laganá and O. Gervasi, *J. Chem. Phys.*, 1993, **99**, 9567.

*Paper* 6/06144C; *Received* 6*th September*, 1996